

FLOW FIELD ANALYSIS INSIDE A THERMAL ENERGY STORAGE DEVICE USING PHASE CHANGE MATERIALS

Roig, F.¹; Egea, A.¹; Crespí-Llorens, D.*²; Vicente, P.²

* Author for correspondence

1. Departamento de Ingeniería Térmica y de Fluidos, Universidad Politécnica de Cartagena.
2. Departamento de Ingeniería Mecánica y Energía, Universidad Miguel Hernández de Elche, Spain,

E-mail: dcrespi@umh.es

ABSTRACT

Thermal energy storage (TES) has recently gained significant attention. The current extensive use of fossil fuel endangers the environment, what implies the necessity of substituting it for the use of renewable energies. However, many renewable energies cannot be produced on demand. Energy needs to be used when produced or, alternatively, stored until it is needed. Among the different TES technologies, phase change materials (PCMs) have been used in the thermal storage of solar energy. However, PCMs, which change phase to solid when discharged, present a high thermal resistance in solid state, limiting the rate of discharge of energy. One way to overcome this problem is the use of active heat transfer enhancement techniques, which consist of the elimination of the solid layer of the PCM created on the heat exchange surface. Therefore, scraped surface heat exchangers (SSHE) represent a promising technology for latent thermal energy store (LTES), which can then be released to a heat transport fluid. In SSHE, power and energy release can be controlled by varying the scraping velocity.

This work presents a study of the flow dynamics of a SSHE in order to characterize the system under different scraping regimes. Particle Image Velocimetry (PIV) and numerical simulation are used to characterize the flow pattern inside the heat exchanger.

The device consists of a PCM tank where energy is stored. Around the PCM tank, water flows through an annular space. This water is used as heat transport fluid which will charge or discharge the PCM used for thermal storage. Inside the PCM tank, a rotating scraper has been installed, in order to remove the solid layer which is formed in the heat exchanger surface in the discharge process. This study focuses on the flow effect produced by the rotating blade in the flow for different working regimes.

INTRODUCTION

The economic development has led to higher demands for energy supply in the world. For that reason, the uses of renewable energies, have experienced significant growth in the last years [9]. Because of the intermittency of renewable energies, the development of thermal energy storage technologies (Ther-

NOMENCLATURE

g	gravity acceleration
p	Pressure
t	Time
u	Drag velocity
v	Absolute fluid velocity
v_r	Relative fluid velocity
v_r^*	Dimensionless relative fluid velocity
k	Turbulent kinetic energy
x	Position
Γ_ϕ	the diffusion of ϕ
G_ϕ, Y_ϕ	terms for production and dissipation of ϕ
D_ω	cross diffusion term

Special characters

ρ	Fluid density
Ω	Scraper rotational velocity
μ_t	Turbulent viscosity
ω	Turbulent dissipation ratio
$\bar{\phi}, \phi'$	Mean and fluctuating components of a fluid variable
Re	Reynolds number
Ta	Taylor number

Subscripts

$i, j, k,$	Coordinate system directions
N	Nominal
r	Relative
tip	At the tip of the scraping blade
ϕ	Generic fluid magnitude

mal Energy Storage, TES) has been given much attention. To that aim, Phase Change Materials (PCM) result in an attractive solution, as they provide high density energy storage.

However, heat transfer processes with PCM usually present two serious drawbacks: a low thermal conductivity and the solidification of the PCM at the heat transfer surface, when the system is discharged, which causes a dramatic drop of heat transfer rates. To overcome this, heat transfer enhancement techniques are required [10]. They can be classified into two general categories: active and passive heat enhancement methods [4]. The advantage of active techniques which scrape the heat transfer surface is obvious, as they remove the solidified PCM from the surface and, thus, they maintain a higher heat transfer rate. Furthermore, usually the movement increases the convection effect, producing a further enhancement. Such techniques have been successfully used for ice slurry production and fouling removal in food pro-

duction, where considerable enhancements have been reported [11; 5; 12]. However, there are very few studies on its suitability for PCM applications.

Maruoka et al. [13] tested a rotative heat exchanger with an inorganic PCM and demonstrated the relation between rotation velocity and heat release. The experiments showed a six times increase in the heat release rate compared to no rotation mode. The heat release was accelerated in the rotation mode, up to 80% of latent heat was released in a short period (15 min). In contrast, the system with no scraping was only capable of extracting 50% of total latent heat after 4 h. Nepustil et al. [14] designed a novel plate heat exchanger for PCM where the heat transfer surface was scraped by linear action. Tombrink et al. [21] studied experimentally a rotating drum heat exchanger for LTES where the heat transfer walls were continuously scraped in order to minimize the layer thickness of the solidified PCM and maximize heat transfer. In that way, the authors were also able to control the thermal power output. Although their prototype was tested with a low melting point fatty acid (decanoic acid), a new experimental test rig for high-temperature applications is being developed. The future experimental research will be supported by their numerical model [20].

Regarding the existing flow patterns in rotatory SSHEs, Trommelen et al. [22] and Härröd [7; 8] studied the influence of the operating conditions of the rotor in the flow. Both conducted experimental studies concluding the internal flow was either a laminar shear flow (Couette flow) or a flow with large toroidal vortices formed in pairs with opposite directions known as Taylor vortices. With increasing rotating speed, the stationary vortices tend to disappear, and the flow pattern becomes fully turbulent [6; 15; 16]. A more detailed study on the velocity field was conducted by Baccar et al. [2; 3]. They performed numerical simulations observing the stagnation of the flow right after the scraper blade. These results agree with the CFD simulations of Stranzinger et al. [17; 18], Yataghene et al. [23; 24] and Sun et al. [19].

In this work, the flow field produced by a rotating scraper in a scraped surface heat exchanger prototype for heat energy storage is analysed. Using Paraffin RT44HC PCM as working fluid, a numerical study has been carried out for different working conditions. Furthermore, an experimental setup has been built to support the conclusions of the model and preliminary experimental results are presented as well. The results of heat release rate under the different conditions show the great potential of the SSHE with PCM for different applications.

EXPERIMENTAL SETUP AND PROCEDURE

This section describes the device under study, the experimental facility and the methodology which has been employed.

As stated before, a prototype has been designed to serve as a high density energy storage. The device is shown in Figure 1, and it mainly consists of two concentric tanks with a rotating surface scraper installed in the inner tank. The scraper has six arms as shown in the figure. The inner tank is filled with PCM

and water flows through the annular space between tanks, serving as heat transfer fluid (HTM). The HTM can be used to charge or discharge the device.

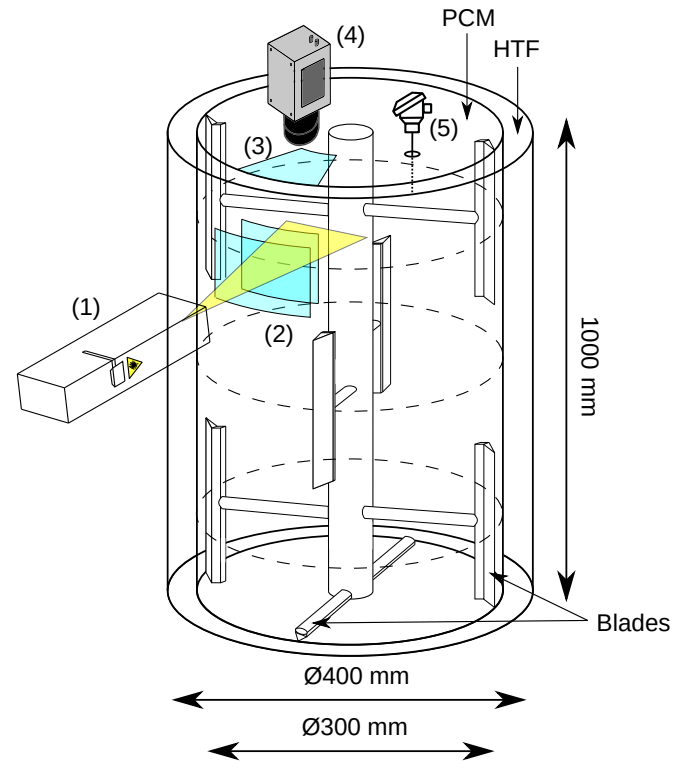


Figure 1. Energy storage device and experimental set-up.

Particle Image Velocimetry (PIV) has been used to obtain the flow pattern of the liquid PCM in a horizontal plane located at 666 mm from the bottom of the tank (being the tank 1 m high) in isothermal conditions. The flow is illuminated by a horizontal laser light sheet produced by a 808 nm Oxford Laser. The laser (1) is able to illuminate the fluid through two aligned windows (2) on the tank wall. Besides, the flow is seeded with 50 μm polyamide particles. A third window (3) in the tank top allows a high speed Motion Scope M3 camera (4) to capture two consecutive pictures of the illuminated particles when triggered. It is triggered by a photoelectric sensor, which detects the scraper. In this way, pictures pairs are taken at the same instant of consecutive cycles. Thus, the flow pattern is obtained by applying the PIV algorithm for 30 pairs of images.

NUMERICAL METHOD

The numerical simulations will be performed by applying the Computational Fluid Dynamics (CFD) to the fluid problem inside the SSHE. To that aim, Fluent 17.1.0 will be used. The energy balance is decoupled from the fluid mechanics of the flow because of the isothermal conditions, avoiding the need to solve the energy equation. Equations 1 and 2 show the expressions for the conservation laws of mass and momentum, respectively,

particularized for the case of an incompressible fluid.

$$\nabla \vec{v} = 0 \quad (1)$$

$$\frac{d}{dt}(\rho \vec{v}) + \nabla(\rho \vec{v} \vec{v}) = -\nabla p + \mu \nabla^2 \vec{v} + \vec{v} + \rho \vec{g} \quad (2)$$

The Moving Reference Frame (MRF) method is used for simulating the rotation of the scraper, because of its lower computational cost when compared to the Sliding Mesh method, and its extended use among the researchers studying SSHEs using CFD. The application of a pure rotating reference frame to the problem leads to a definition of the relative velocity v_r of the flow seen from this reference frame as the combination of the absolute velocity of the fluid and the rotating speed of the reference frame. Equations 3 and 4 show the expressions defining the relationship between both reference frames.

$$\vec{v}_r = \vec{v} - \vec{u} \quad (3)$$

$$\vec{u} = \vec{\Omega} \times \vec{r} \quad (4)$$

The governing equations of the system can be written now considering the rotating reference frame by substituting the absolute velocity for relative velocity, obtaining the equations 5 and 6. Note that two terms are added to the momentum equation: the Coriolis acceleration $2\vec{\Omega} \times \vec{v}_r$ and the centripetal acceleration $\vec{\Omega} \times \vec{\Omega} \times \vec{r}$.

$$\nabla \vec{v}_r = 0 \quad (5)$$

$$\frac{d}{dt}(\rho \vec{v}_r) + \nabla(\rho \vec{v}_r \vec{v}_r) = -\nabla p + \mu \nabla^2 \vec{v}_r + \rho \vec{g} - \rho(2\vec{\Omega} \times \vec{r} + \vec{\Omega} \times \vec{\Omega} \times \vec{r}) \quad (6)$$

Regarding the turbulence modeling of the flow, it is assumed that the isothermal monophasic flow of the PCM would be dominated by the rotation of the scraper blades, leading to the possible formation of a secondary vortex flow. Hence, the k- ω Shear Stress Transport (SST) model is proposed in order to properly simulate the flow. It is a Reynolds Average Navier-Stokes (RANS) model which combines both the k- ϵ and k- ω models through a blending function, taking advantage of the numerical features for free flow and near wall regions respectively. This model adds two additional transport equations for the calculation of the Reynolds stresses derived from the decomposition of the fluid magnitudes into mean and fluctuating components ($\phi = \bar{\phi} + \phi'$) as part of the Reynolds Averaging method. Considering a single component $\{i, j, k\}$ of the velocity magnitude for

simplicity, equation 7 shows the term added to the momentum equation 2 due to the turbulence model, which depends on the turbulent kinetic energy k and the turbulent viscosity μ_t . In the k- ω SST model, μ_t is obtained as a relationship between k and the turbulent dissipation ratio ω .

$$-\rho \overline{v'_i v'_j} = \mu_t \left(\frac{\partial v_i}{\partial x_j} + \frac{\partial v_j}{\partial x_i} \right) - \frac{2}{3} \left(\rho k + \mu_t \frac{\partial v_k}{\partial x_k} \right) \delta_{ij} \quad (7)$$

Equations 8 and 9 present the additional transport equations, where Γ_ϕ is the diffusion of ϕ ; G_ϕ and Y_ϕ are the terms for production and dissipation of ϕ ; and D_ω is the cross diffusion term added to the transport equation of ω as a result of merging k- ϵ and k- ω models. The authors refer to the available information in the Fluent Theory Guide [1] for further details about the implementation of the k- ω SST model.

$$\frac{\partial}{\partial t}(\rho k) + \frac{\partial}{\partial x_i}(\rho k v_i) = \frac{\partial}{\partial x_j} \left(\Gamma_k \frac{\partial k}{\partial x_j} \right) + G_k - Y_k \quad (8)$$

$$\frac{\partial}{\partial t}(\rho \omega) + \frac{\partial}{\partial x_i}(\rho \omega v_i) = \frac{\partial}{\partial x_j} \left(\Gamma_\omega \frac{\partial \omega}{\partial x_j} \right) + G_\omega - Y_\omega + D_\omega \quad (9)$$

The computational domain is discretized with an unstructured 3D mesh developed from the fluid volume created by subtraction of the computational-aided design (CAD) model of the SSHE. The lack of axisymmetry due to the distribution of the scraper blades and the effect of gravity along the height of the SSHE force to treat the problem as three-dimensional. It is not possible either to use a periodic control volume. In order to mitigate the expensive computational cost expected from these simulations, the existing gap between the blade tip and the containment shell is neglected, giving the fact that the scope of this work concerns the study of the flow pattern and velocity fields in the SSHE from a macroscopic standpoint. Furthermore, the high computational cost limits the density of the mesh. Hence, a mesh comprised of 10.5 million elements will be used for the simulations after verifying the relative error on velocity magnitude relies on around 10% for the primary flow when compared to finer meshes, showing good agreement in the contour shapes. However, it won't be possible to study in detail the secondary flows because the mesh is not fine enough to properly capture the vortex formation.

With regard to the boundary conditions, a stationary non-slip condition will be placed in all containment walls, while the scraper will be a moving non-slip wall at rotating speed Ω , equal to the rotating speed of the reference frame. Furthermore, although the flow inside the SSHE should be periodic when considering the isothermal condition, transient simulations will be performed with the intention of assessing the variation of the secondary flow over time.

For the spatial discretization of the governing equations, an upwind second order scheme is selected for the calculation of

fluid magnitudes. The gradients are calculated by the least squares method, and a second order temporal discretization is also selected. The pressure-based solver is applied to solve the linearized system of governing equations. For the pressure-velocity coupling, the SIMPLE algorithm will be used.

RESULTS

Numerical simulations

In order to characterize the flow pattern inside the SSHE, numerical simulations are conducted for the nominal rotating speed $\Omega_N = 7.46$ rpm ($Re_r = 1.6 \cdot 10^4$, $Ta = 1228$) as well as for other two proportional rotating speeds: $0.5\Omega_N$ ($Re_r = 8 \cdot 10^3$, $Ta = 614$) and $1.5\Omega_N$ ($Re_r = 2.4 \cdot 10^4$, $Ta = 1842$). The study will be focused on the assessment of the relative velocity field for different sections of the fluid volume, as the resulting contours allow a better understanding of the flow pattern when compared to the absolute reference frame. This is equivalent to consider that the scraper remains still while the flow moves within the domain, rotating clockwise around the shaft. In addition, the relative velocity is non-dimensionalized by the maximum velocity (the velocity at the scraper tip u_{tip}) to be able to compare the results obtained from the simulations at different rotating speeds. Equation 10 shows the expression for calculating the dimensionless relative velocity v_r^* .

$$v_r^* = \frac{v_r}{u_{tip}} = \frac{v_r}{\Omega r_{tip}} \quad (10)$$

Some general appreciations can be made based on the velocity field when operating at nominal speed. Figure 2 shows the relative velocity field contours for different sections of the fluid volume, focusing on the most representative areas: the middle section of each module of blades (planes 2, 4 and 6), the transition area between the modules (planes 3 and 5) and the bottom zone (plane 1). The similarities between the planes $\{2,4,6\}$ and $\{3,5\}$ indicate the flow is dominated by the in-plane forces derived from the rotation of the scraper, hence concluding the effects of the gravity forces are negligible for the flow pattern formation in the case of isothermal flow. Regarding the values for the velocity field, the maximum relative velocities are located on the lateral walls and equal to u_{tip} following the non-slip condition, while the minimum values can be found in the area surrounding the shaft also following the non-slip boundary condition.

By observing the middle sections, it can be stated that the flow inside the SSHE is predominantly laminar, as shown by the concentric contours of velocity typical from the shear flows. The flow near the container walls is accelerated by the scraper blade, reaching velocities around $0.65u_{tip}$. Once the flow detaches from the blade, it loses speed and the pressure drop generated at the back of the blade forces the formation of a roll-up vortex, generating the secondary flow represented by the contours of $v_r^* < 0.25$. Although some kind of Taylor vortex seem to be forming when observing longitudinal section planes at the back of the

blades, the lack of resolution of the mesh in the secondary flow field area prevents us from conducting a detailed study. On the other hand, the rest of the flow which is not directly affected by the blades rotates at a much lower speed, forming a bulk volume of $v_r^* < 0.25$ around the shaft. In this region, the movement is transmitted thanks to the variation on shear forces between the zones rotating at different speeds.

Although the flow pattern is common for all sections, the formation of the secondary flow varies depending on the area that is considered. The secondary flow reaches its maximum extension at the middle section of the modules, while at the transition zones between modules its existence is nearly negligible. Especial mention needs to be made for the bottom area where, in addition to the blade secondary flow, another secondary flow is generated from the bottom scraper.

The flow pattern observed for the operation at nominal rotating speed is also present in the simulations conducted for $0.5\Omega_N$ and $1.5\Omega_N$ as shown in Figure 3. In fact, it can be affirmed the flow regimen inside the SSHE is the same for $\Omega \in [0.5\Omega_N, 1.5\Omega_N]$: a periodic laminar rotating flow with secondary vortex flows at the back of the blades. It can be assumed that a much lower rotating speed would be needed in order to see the transition from fully laminar flow to the Taylor vortex flow. However, there are slight alterations of the flow pattern derived from the increase of rotating speed. The relevance of the inertial forces increases over the viscous forces, reducing the magnitude of the accelerated flow and increasing the velocity gradient from the lateral wall to the low speed bulk volume surrounding the shaft.

Preliminary Experimental results

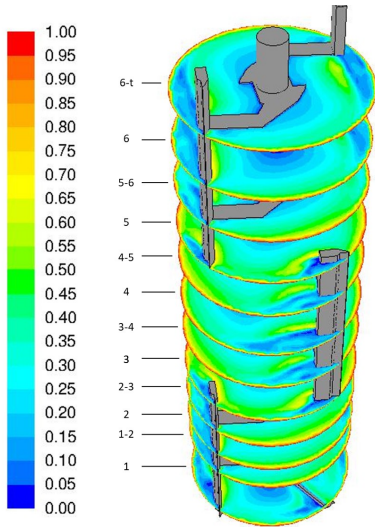
This section shows the preliminary experimental results of the inner tank flow field. Figure 4 shows the area downstream the scraper, where a wake of high flow velocities is detected due to the movement of the scraper. Besides, vortex formation is also observed, in accordance with numerical results.

CONCLUSION

This work presents the experimental setup built to analyze the flow pattern in a novel heat storage system. The system has been built to obtain it by using PIV technique. From the numerical simulations, it can be confirmed the flow inside the SSHE is predominantly laminar when operating at nominal speed. The flow pattern is dominated by the in-plane forces derived from the rotation of the blades, being the contribution of gravity forces negligible. However, secondary flows appear at the back of the blades due to the roll-up vortex formed after the accelerated flow detaches from the blades. It can also be stated that this flow pattern remains unaltered for a wide operating range around the nominal speed $\Omega \in [0.5\Omega_N, 1.5\Omega_N]$.

The preliminary experimental results support the numerical simulations. The experimental study will be carried out further to fully validate the numerical model and provide additional information.

The conclusions obtained for the behavior of the internal flow



(a) Distribution of planes along the SSHE

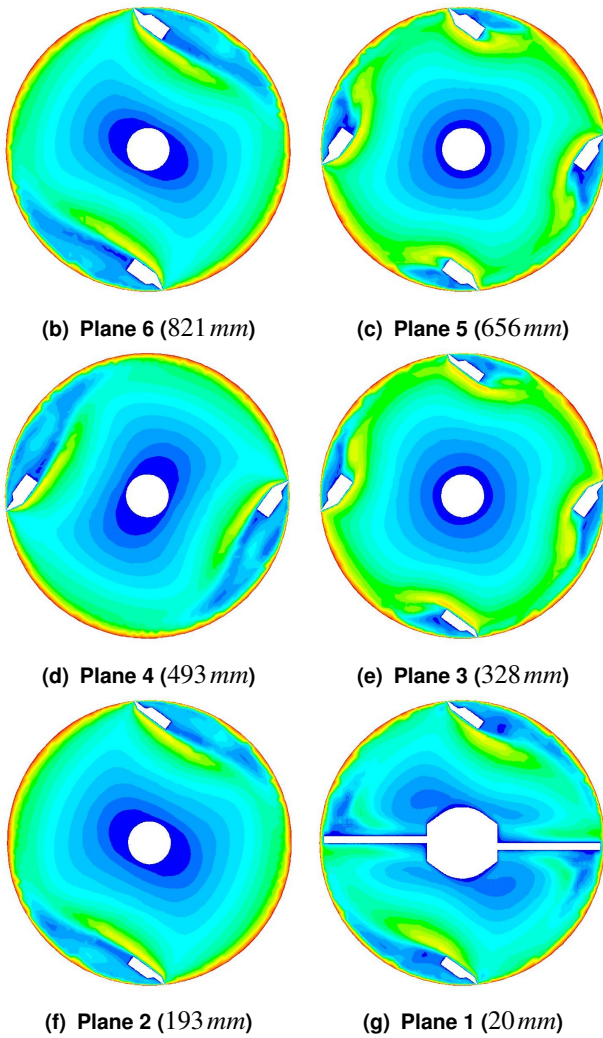


Figure 2. Contours of dimensionless relative velocity v_r^* for nominal rotating speed Ω_N .

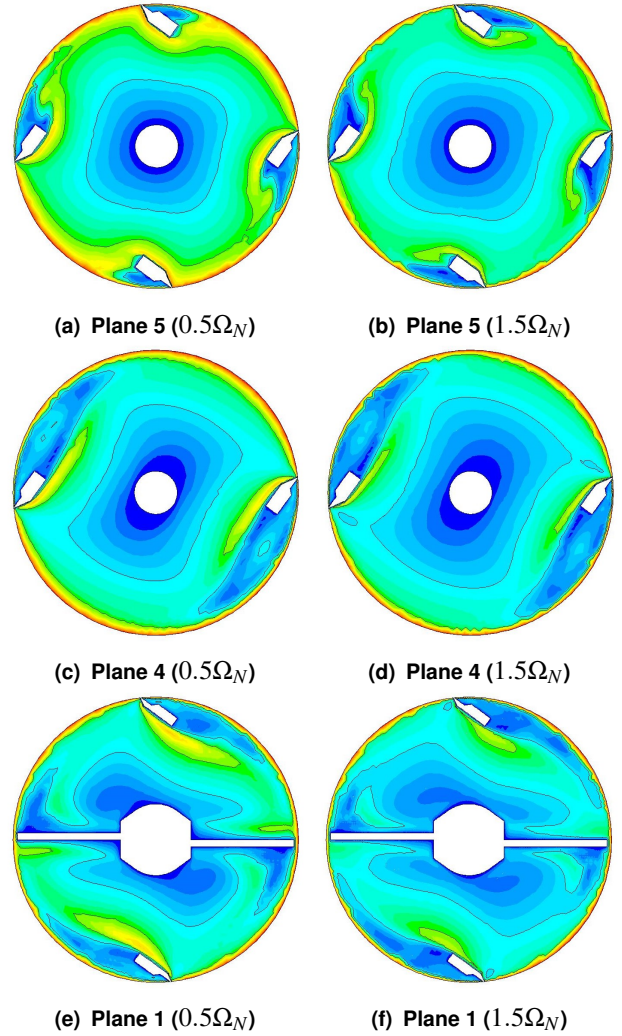
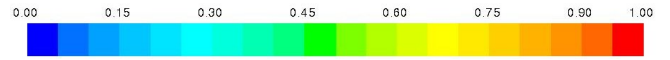


Figure 3. Contours of dimensionless relative velocity v_r^* for $0.5\Omega_N$ and $1.5\Omega_N$.

of the SSHE will have considerable value on the future optimization of the heat transfer in the system.

ACKNOWLEDGMENT

The authors gratefully acknowledge the financial support of the project ALTES: "Active Latent Thermal Energy Storage", Ref. PGC2018-100864-B-C21 and PGC2018-100864-A-C22 by MCIN/AEI/ 10.13039/501100011033 and by "ERDF A way of making Europe".

REFERENCES

- [1] ANSYS *Fluent Theory Guide*. ANSYS, Inc., release 15.0 edition, 2013.
- [2] Mounir Baccar and Mohamed Salah Abid. Numerical analysis of three-dimensional flow and thermal behaviour in a

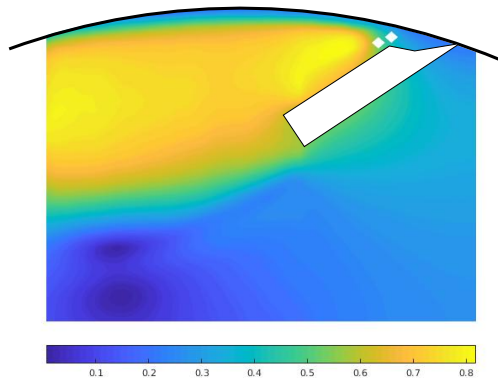


Figure 4. PIV results of normalized velocity for rated rotation speed.

- scraped-surface heat exchanger. *Revue générale de thermique*, 36(10):782–790, 1997.
- [3] Mounir Baccar and Mohamed Salah Abid. Simulation numérique des comportements hydrodynamiques et thermiques des échangeurs racleurs opérant en régime turbulent. *International journal of thermal sciences*, 38(7):634–644, 1999.
- [4] Arthur E Bergles. Recent developments in enhanced heat transfer. *Heat and Mass Transfer*, 47(8):1001, 2011.
- [5] D. Crespi-Llorens, P. Martínez, P. Vicente, and A. Viedma. Effect of the axial scraping velocity on enhanced heat exchangers. *International Journal of Heat and Fluid Flow*, 44:265–275, 2013. Cited By :5.
- [6] Eric Dumont, Francine Fayolle, and Jack Legrand. Flow regimes and wall shear rates determination within a scraped surface heat exchanger. *Journal of Food Engineering*, 45(4):195–207, 2000.
- [7] Magnus Härröd. Scraped surface heat exchangers: A literature survey of flow patterns, mixing effects, residence time distribution, heat transfer and power requirements. *Journal of Food Process Engineering*, 9(1):1–62, 1986.
- [8] Magnus Härröd. Methods to distinguish between laminar and vortical flow in scraped surface heat exchangers. *Journal of Food Process Engineering*, 13(1):39–57, 1990.
- [9] Alireza Jaber Khosroshahi and Siamak Hossainpour. Investigation of storage rotation effect on phase change material charging process in latent heat thermal energy storage system. *Journal of Energy Storage*, 36(September 2020):102442, 2021.
- [10] Ramin Karami and Babak Kamkari. Experimental investigation of the effect of perforated fins on thermal performance enhancement of vertical shell and tube latent heat energy storage systems. *Energy Conversion and Management*, 210(November 2019):112679, 2020.
- [11] Mohamed Ben Lakhdar, Rosalia Cerecero, Graciela Alvarez, Jacques Guilpart, Denis Flick, and André Lallemand. Heat transfer with freezing in a scraped surface heat exchanger. *Applied Thermal Engineering*, 25(1):45–60, 2005.
- [12] D. S. Martínez, J. P. Solano, P. G. Vicente, and A. Viedma. Flow pattern analysis in a rotating scraped surface plate heat exchanger. *Applied Thermal Engineering*, 160(May):113795, 2019.
- [13] Nobuhiro Maruoka, Taichi Tsutsumi, Akihisa Ito, Miho Hayasaka, and Hiroshi Nogami. Heat release characteristics of a latent heat storage heat exchanger by scraping the solidified phase change material layer. *Energy*, 205:118055, 2020.
- [14] Ulrich Nepustil, Doerte Laing-Nepustil, Detlev Lodemann, Rameesh Sivabalan, and Volker Hausmann. High Temperature Latent Heat Storage with Direct Electrical Charging – Second Generation Design. *Energy Procedia*, 99:314–320, 2016.
- [15] Sanjay B Pawar and BN Thorat. Cfd simulation of taylor-couette flow in scraped surface heat exchanger. *Chemical Engineering Research and Design*, 90(3):313–322, 2012.
- [16] Oliver Richter, Heike Hoffmann, and Bettina Kraushaar-Czarnetzki. Effect of the rotor shape on the mixing characteristics of a continuous flow taylor-vortex reactor. *Chemical Engineering Science*, 63(13):3504–3513, 2008.
- [17] M Stranzinger, A Bieder, K Feigl, and E Windhab. Effects of flow incidence and secondary mass flow rate on flow structuring contributions in scraped surface heat exchangers. *Journal of food process engineering*, 25(3):159–187, 2002.
- [18] M Stranzinger, K Feigl, and E Windhab. Non-newtonian flow behaviour in narrow annular gap reactors. *Chemical engineering science*, 56(11):3347–3363, 2001.
- [19] K-H Sun, DL Pyle, AD Fitt, CP Please, Mike J Baines, and N Hall-Taylor. Numerical study of 2d heat transfer in a scraped surface heat exchanger. *Computers & Fluids*, 33(5-6):869–880, 2004.
- [20] Jonas Tombrink and Dan Bauer. Simulation of a rotating drum heat exchanger for latent heat storage using a quasi-stationary analytical approach and a numerical transient finite difference scheme. *Applied Thermal Engineering*, 194(May):117029, 2021.
- [21] Jonas Tombrink, Henning Jockenhöfer, and Dan Bauer. Experimental investigation of a rotating drum heat exchanger for latent heat storage. *Applied Thermal Engineering*, 183(October 2020), 2021.
- [22] AM Trommelen and WJ Beek. Flow phenomena in a scraped-surface heat exchanger (“votator”-type). *Chemical Engineering Science*, 26(11):1933–1942, 1971.
- [23] Mourad Yataghene and Jack Legrand. A 3d-cfd model thermal analysis within a scraped surface heat exchanger. *Computers & Fluids*, 71:380–399, 2013.
- [24] Mourad Yataghene, Jérémy Pruvost, Francine Fayolle, and Jack Legrand. Cfd analysis of the flow pattern and local shear rate in a scraped surface heat exchanger. *Chemical Engineering and Processing: Process Intensification*, 47(9-10):1550–1561, 2008.